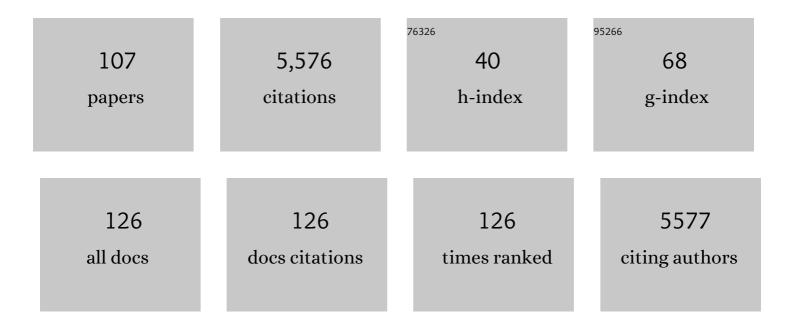
List of Publications by Year in descending order

Source: https://exaly.com/author-pdf/2643602/publications.pdf Version: 2024-02-01



Μλακιίς Βλάτη

#	Article	IF	CITATIONS
1	Simultaneous multislice (SMS) imaging techniques. Magnetic Resonance in Medicine, 2016, 75, 63-81.	3.0	420
2	Three dimensional echo-planar imaging at 7 Tesla. NeuroImage, 2010, 51, 261-266.	4.2	266
3	High-Resolution MR Venography at 3.0 Tesla. Journal of Computer Assisted Tomography, 2000, 24, 949-957.	0.9	190
4	Layerâ€specific BOLD activation in human V1. Human Brain Mapping, 2010, 31, 1297-1304.	3.6	190
5	Magnetic susceptibility-weighted MR phase imaging of the human brain. American Journal of Neuroradiology, 2005, 26, 736-42.	2.4	181
6	Fast quantitative susceptibility mapping using 3D EPI and total generalized variation. Neurolmage, 2015, 111, 622-630.	4.2	157
7	Multi-echo fMRI of the cortical laminae in humans at 7T. NeuroImage, 2011, 56, 1276-1285.	4.2	152
8	A cortical vascular model for examining the specificity of the laminar BOLD signal. NeuroImage, 2016, 132, 491-498.	4.2	136
9	Nonnvasive assessment of vascular architecture and function during modulated blood oxygenation using susceptibility weighted magnetic resonance imaging. Magnetic Resonance in Medicine, 2005, 54, 87-95.	3.0	130
10	Evaluation of preoperative high magnetic field motor functional MRI (3 Tesla) in glioma patients by navigated electrocortical stimulation and postoperative outcome. Journal of Neurology, Neurosurgery and Psychiatry, 2005, 76, 1152-1157.	1.9	125
11	Memory stabilization with targeted reactivation during human slow-wave sleep. Proceedings of the National Academy of Sciences of the United States of America, 2012, 109, 10575-10580.	7.1	121
12	Power independent of number of slices (PINS) radiofrequency pulses for lowâ€power simultaneous multislice excitation. Magnetic Resonance in Medicine, 2011, 66, 1234-1240.	3.0	110
13	Magnetic Resonance Imaging Contrast Enhancement of Brain Tumors at 3 Tesla Versus 1.5 Tesla. Investigative Radiology, 2002, 37, 114-119.	6.2	107
14	MR venography of the human brain using susceptibility weighted imaging at very high field strength. Magnetic Resonance Materials in Physics, Biology, and Medicine, 2008, 21, 149-158.	2.0	107
15	Linear reconstruction of perceived images from human brain activity. Neurolmage, 2013, 83, 951-961.	4.2	103
16	Automated unwrapping of MR phase images applied to BOLD MR-venography at 3 Tesla. Journal of Magnetic Resonance Imaging, 2003, 18, 175-180.	3.4	98
17	Sleep Supports Selective Retention of Associative Memories Based on Relevance for Future Utilization. PLoS ONE, 2012, 7, e43426.	2.5	96
18	Wavelet-based multifractal analysis of fMRI time series. NeuroImage, 2004, 22, 1195-1202.	4.2	89

#	Article	IF	CITATIONS
19	A quantitative comparison of functional MRI cluster analysis. Artificial Intelligence in Medicine, 2004, 31, 57-71.	6.5	84
20	DeepQSM - using deep learning to solve the dipole inversion for quantitative susceptibility mapping. NeuroImage, 2019, 195, 373-383.	4.2	84
21	Phase unwrapping of MR images using ΦUN – A fast and robust region growing algorithm. Medical Image Analysis, 2009, 13, 257-268.	11.6	82
22	7 tesla MRI of microbleeds and white matter lesions as seen in vascular dementia. Journal of Magnetic Resonance Imaging, 2011, 33, 782-791.	3.4	74
23	Influence of fMRI smoothing procedures on replicability of fine scale motor localization. NeuroImage, 2005, 24, 323-331.	4.2	71
24	Contrast-to-noise ratio (CNR) as a quality parameter in fMRI. Journal of Magnetic Resonance Imaging, 2007, 25, 1263-1270.	3.4	71
25	Generic acquisition protocol for quantitative MRI of the spinal cord. Nature Protocols, 2021, 16, 4611-4632.	12.0	65
26	Serial correlations in single-subject fMRI with sub-second TR. NeuroImage, 2018, 166, 152-166.	4.2	61
27	Robust field map generation using a triple-echo acquisition. Journal of Magnetic Resonance Imaging, 2004, 20, 730-734.	3.4	59
28	Diffusion tensor characteristics of gyrencephaly using high resolution diffusion MRI in vivo at 7T. NeuroImage, 2015, 109, 378-387.	4.2	59
29	Improved sensitivity and specificity for resting state and task fMRI with multiband multi-echo EPI compared to multi-echo EPI at 7 T. NeuroImage, 2015, 119, 352-361.	4.2	58
30	A method for the dynamic correction of B 0 -related distortions in single-echo EPI at 7 T. NeuroImage, 2018, 168, 321-331.	4.2	57
31	High-Resolution Three-Dimensional Contrast-Enhanced Blood Oxygenation Level-Dependent Magnetic Resonance Venography of Brain Tumors at 3 Tesla: First Clinical Experience and Comparison with 1.5 Tesla. Investigative Radiology, 2003, 38, 409-414.	6.2	56
32	Whole brain, high resolution spin-echo resting state fMRI using PINS multiplexing at 7T. NeuroImage, 2012, 62, 1939-1946.	4.2	56
33	Echo timeâ€dependent quantitative susceptibility mapping contains information on tissue properties. Magnetic Resonance in Medicine, 2017, 77, 1946-1958.	3.0	56
34	High-resolution, multiple gradient-echo functional MRI at 1.5 T. Magnetic Resonance Imaging, 1999, 17, 321-329.	1.8	54
35	Layer-specific diffusion weighted imaging in human primary visual cortex inÂvitro. Cortex, 2013, 49, 2569-2582.	2.4	54
36	Scaling laws and persistence in human brain activity. Physica A: Statistical Mechanics and Its Applications, 2003, 326, 511-521.	2.6	53

#	Article	IF	CITATIONS
37	T1 mapping of the entire lung parenchyma: Influence of the respiratory phase in healthy individuals. Journal of Magnetic Resonance Imaging, 2005, 21, 759-764.	3.4	53
38	T1 mapping of the entire lung parenchyma: Influence of respiratory phase and correlation to lung function test results in patients with diffuse lung disease. Magnetic Resonance in Medicine, 2008, 59, 96-101.	3.0	51
39	MR Contrast Agent at High-Field MRI (3 Tesla). Topics in Magnetic Resonance Imaging, 2003, 14, 365-375.	1.2	50
40	Diffusion parameter mapping with the combined intravoxel incoherent motion and kurtosis model using artificial neural networks at 3ÂT. NMR in Biomedicine, 2017, 30, e3833.	2.8	49
41	Combining phase images from array coils using a short echo time reference scan (COMPOSER). Magnetic Resonance in Medicine, 2017, 77, 318-327.	3.0	49
42	Functional connectivity during light sleep is correlated with memory performance for face–location associations. NeuroImage, 2011, 57, 262-270.	4.2	46
43	Measuring the effects of attention to individual fingertips in somatosensory cortex using ultra-high field (7T) fMRI. Neurolmage, 2017, 161, 179-187.	4.2	45
44	Contrast-Enhanced, High-Resolution, Susceptibility-Weighted Magnetic Resonance Imaging of the Brain. Investigative Radiology, 2006, 41, 249-255.	6.2	42
45	Application of PINS radiofrequency pulses to reduce power deposition in RARE/turbo spin echo imaging of the human head. Magnetic Resonance in Medicine, 2014, 71, 44-49.	3.0	42
46	Whole brain, high resolution multiband spin-echo EPI fMRI at 7T: A comparison with gradient-echo EPI using a color-word Stroop task. NeuroImage, 2014, 97, 142-150.	4.2	42
47	Bayesian population receptive field modeling in human somatosensory cortex. NeuroImage, 2020, 208, 116465.	4.2	41
48	Fuzzy cluster analysis of high-field functional MRI data. Artificial Intelligence in Medicine, 2003, 29, 203-223.	6.5	40
49	Generalized iNverse imaging (GIN): Ultrafast fMRI with physiological noise correction. Magnetic Resonance in Medicine, 2013, 70, 962-971.	3.0	40
50	Very high-resolution three-dimensional functional MRI of the human visual cortex with elimination of large venous vessels. NMR in Biomedicine, 2007, 20, 477-484.	2.8	38
51	Susceptibility weighted magnetic resonance imaging of cerebral cavernous malformations: prospects, drawbacks, and first experience at ultra–high field strength (7-Tesla) magnetic resonance imaging. Neurosurgical Focus, 2010, 29, E5.	2.3	38
52	Improved elimination of phase effects from background field inhomogeneities for susceptibility weighted imaging at high magnetic field strengths. Magnetic Resonance Imaging, 2008, 26, 1145-1151.	1.8	37
53	Functional MRI of the human motor cortex using single-shot, multiple gradient-echo spiral imaging. Magnetic Resonance Imaging, 1999, 17, 1239-1243.	1.8	35
54	<i>T</i> ₂ -weighted 3D fMRI using <i>S</i> ₂ -SSFP at 7 tesla. Magnetic Resonance in Medicine, 2010, 63, 1015-1020.	3.0	34

#	Article	IF	CITATIONS
55	Referenceâ€free unwarping of EPI data using dynamic offâ€resonance correction with multiecho acquisition (DOCMA). Magnetic Resonance in Medicine, 2012, 68, 1247-1254.	3.0	32
56	Using multi-echo simultaneous multi-slice (SMS) EPI to improve functional MRI of the subcortical nuclei of the basal ganglia at ultra-high field (7T). NeuroImage, 2018, 172, 886-895.	4.2	32
57	Electrophysiological Correlation Patterns of Resting State Networks in Single Subjects: A Combined EEG–fMRI Study. Brain Topography, 2013, 26, 98-109.	1.8	31
58	An Investigation of RSN Frequency Spectra Using Ultra-Fast Generalized Inverse Imaging. Frontiers in Human Neuroscience, 2013, 7, 156.	2.0	30
59	New acquisition techniques and their prospects for the achievable resolution of fMRI. Progress in Neurobiology, 2021, 207, 101936.	5.7	27
60	Open-access quantitative MRI data of the spinal cord and reproducibility across participants, sites and manufacturers. Scientific Data, 2021, 8, 219.	5.3	27
61	Explorative signal processing in functional MR imaging. International Journal of Imaging Systems and Technology, 1999, 10, 166-176.	4.1	26
62	Assessment of microstructural signal compartments across the corpus callosum using multi-echo gradient recalled echo at 7ÂT. NeuroImage, 2018, 182, 407-416.	4.2	26
63	Singleâ€shot echoâ€planar imaging with Nyquist ghost compensation: Interleaved dual echo with acceleration (IDEA) echoâ€planar imaging (EPI). Magnetic Resonance in Medicine, 2013, 69, 37-47.	3.0	23
64	Cued reactivation during slow-wave sleep induces brain connectivity changes related to memory stabilization. Scientific Reports, 2018, 8, 16958.	3.3	23
65	SHARQnet – Sophisticated harmonic artifact reduction in quantitative susceptibility mapping using a deep convolutional neural network. Zeitschrift Fur Medizinische Physik, 2019, 29, 139-149.	1.5	22
66	Advances in High-Field BOLD fMRI. Materials, 2011, 4, 1941-1955.	2.9	21
67	BOLD fMRI signal characteristics of S1- and S2-SSFP at 7 Tesla. Frontiers in Neuroscience, 2014, 8, 49.	2.8	21
68	Correcting dynamic distortions in 7T echo planar imaging using a jittered echo time sequence. Magnetic Resonance in Medicine, 2016, 76, 1388-1399.	3.0	20
69	Modulation of signal changes in gradient-recalled echo functional MRI with increasing echo time correlate with model calculations. Magnetic Resonance Imaging, 1997, 15, 745-752.	1.8	19
70	Improved susceptibility weighted imaging at ultra-high field using bipolar multi-echo acquisition and optimized image processing: CLEAR-SWI. NeuroImage, 2021, 237, 118175.	4.2	19
71	Title is missing!. Investigative Radiology, 2003, 38, 409-414.	6.2	18
72	FMRI reveals functional cortex in a case of inconclusive Wada testing. Clinical Neurology and Neurosurgery, 2005, 107, 147-151.	1.4	18

#	Article	IF	CITATIONS
73	Comparison of fMRI coregistration results between human experts and software solutions in patients and healthy subjects. European Radiology, 2007, 17, 1634-1643.	4.5	18
74	A study-specific fMRI normalization approach that operates directly on high resolution functional EPI data at 7Tesla. NeuroImage, 2014, 100, 710-714.	4.2	18
75	A timeâ€efficient acquisition protocol for multipurpose diffusionâ€weighted microstructural imaging at 7 Tesla. Magnetic Resonance in Medicine, 2017, 78, 2170-2184.	3.0	18
76	7T GRE-MRI signal compartments are sensitive to dysplastic tissue in focal epilepsy. Magnetic Resonance Imaging, 2019, 61, 1-8.	1.8	18
77	Structure Tensor Informed Fiber Tractography (STIFT) by combining gradient echo MRI and diffusion weighted imaging. NeuroImage, 2012, 59, 3941-3954.	4.2	17
78	The Quest for EEG Power Band Correlation with ICA Derived fMRI Resting State Networks. Frontiers in Human Neuroscience, 2013, 7, 315.	2.0	17
79	ECG Triggering in Ultra-High Field Cardiovascular MRI. Tomography, 2016, 2, 167-174.	1.8	17
80	The challenge of biasâ€free coil combination for quantitative susceptibility mapping at ultraâ€high field. Magnetic Resonance in Medicine, 2018, 79, 97-107.	3.0	17
81	Robust SENSE reconstruction of simultaneous multislice EPI with lowâ€rank enhanced coil sensitivity calibration and sliceâ€dependent 2D Nyquist ghost correction. Magnetic Resonance in Medicine, 2018, 80, 1376-1390.	3.0	16
82	Adaptive <scp>SAR</scp> massâ€averaging framework to improve predictions of local <scp>RF</scp> heating near a hip implant for parallel transmit at 7 <scp>T</scp> . Magnetic Resonance in Medicine, 2019, 81, 615-627.	3.0	15
83	Simultaneous multislice inversion contrast imaging using power independent of the number of slices (PINS) and delays alternating with nutation for tailored excitation (DANTE) radio frequency pulses. Magnetic Resonance in Medicine, 2013, 69, 1670-1676.	3.0	14
84	From ultrahigh to extreme field magnetic resonance: where physics, biology and medicine meet. Magnetic Resonance Materials in Physics, Biology, and Medicine, 2016, 29, 309-311.	2.0	14
85	Online decoding of objectâ€based attention using realâ€ŧime f <scp>MRI</scp> . European Journal of Neuroscience, 2014, 39, 319-329.	2.6	13
86	Pulsed arterial spin labelling at ultra-high field with a B 1 + -optimised adiabatic labelling pulse. Magnetic Resonance Materials in Physics, Biology, and Medicine, 2016, 29, 463-473.	2.0	13
87	Non-linear realignment improves hippocampus subfield segmentation reliability. NeuroImage, 2019, 203, 116206.	4.2	13
88	Characterization of BOLD activation in multi-echo fMRI data using fuzzy cluster analysis and a comparison with quantitative modeling. NMR in Biomedicine, 2001, 14, 484-489.	2.8	12
89	Quantification of signal changes in gradient recalled echo FMRI. Magnetic Resonance Imaging, 1997, 15, 753-762.	1.8	11
90	A populationâ€specific symmetric phase model to automatically analyze susceptibilityâ€weighted imaging (SWI) phase shifts and phase symmetry in the human brain. Journal of Magnetic Resonance Imaging, 2010, 31, 215-220.	3.4	11

#	Article	IF	CITATIONS
91	Filtered deconvolution of a simulated and an in vivo phase model of the human brain. Journal of Magnetic Resonance Imaging, 2010, 32, 289-297.	3.4	11
92	Selective channel combination of MRI signal phase. Magnetic Resonance in Medicine, 2016, 76, 1469-1477.	3.0	11
93	PECâ€GRAPPA reconstruction of simultaneous multislice EPI with sliceâ€dependent 2D Nyquist ghost correction. Magnetic Resonance in Medicine, 2019, 81, 1924-1934.	3.0	11
94	Longitudinal Automatic Segmentation of Hippocampal Subfields (LASHiS) using multi-contrast MRI. Neurolmage, 2020, 218, 116798.	4.2	11
95	QSMxT: Robust masking and artifact reduction for quantitative susceptibility mapping. Magnetic Resonance in Medicine, 2022, 87, 1289-1300.	3.0	11
96	Comparison of multi-echo spiral and echo planar imaging in functional MRI. Magnetic Resonance Imaging, 2002, 20, 359-364.	1.8	10
97	Contrast Enhanced Susceptibility Weighted Imaging (CE-SWI) of the Mouse Brain Using Ultrasmall Superparamagnetic Ironoxide Particles (USPIO). Zeitschrift Fur Medizinische Physik, 2006, 16, 269-274.	1.5	10
98	Accelerated mapping of magnetic susceptibility using 3D planesâ€onâ€aâ€paddlewheel (POP) EPI at ultraâ€high field strength. NMR in Biomedicine, 2017, 30, e3620.	2.8	10
99	Improving FLAIR SAR efficiency at 7T by adaptive tailoring of adiabatic pulse power through deep learning estimation. Magnetic Resonance in Medicine, 2021, 85, 2462-2476.	3.0	10
100	Cardiac Magnetic Resonance Imaging at 7 Tesla. Journal of Visualized Experiments, 2019, , .	0.3	7
101	A numerical and experimental study of RF shimming in the presence of hip prostheses using adaptive SAR at 3 T. Magnetic Resonance in Medicine, 2019, 81, 3826-3839.	3.0	6
102	Patient with ALS with a novel TBK1 mutation, widespread brain involvement, behaviour changes and metabolic dysfunction. Journal of Neurology, Neurosurgery and Psychiatry, 2019, 90, 952-954.	1.9	6
103	7-Tesla Functional Cardiovascular MR Using Vectorcardiographic Triggering—Overcoming the Magnetohydrodynamic Effect. Tomography, 2021, 7, 323-332.	1.8	3
104	Modeling and suppression of respiration induced B0-fluctuations in non-balanced steady-state free precession sequences at 7 Tesla. Magnetic Resonance Materials in Physics, Biology, and Medicine, 2013, 26, 377-387.	2.0	2
105	Towards Optimising MRI Characterisation of Tissue (TOMCAT) Dataset including all Longitudinal Automatic Segmentation of Hippocampal Subfields (LASHIS) data. Data in Brief, 2020, 32, 106043.	1.0	2
106	Influence of 7T GRE-MRI Signal Compartment Model Choice on Tissue Parameters. Frontiers in Neuroscience, 2020, 14, 271.	2.8	2
107	Field strength influences on gradient recalled echo MRI signal compartment frequency shifts. Magnetic Resonance Imaging, 2020, 70, 98-107.	1.8	1